Reconstruction of 1d Emission Profile from 2d Synthetic Plasma Image

Student Name: Dhruvil Gorasiya
Enrollment ID: **201901061**
B. Tech. Project (BTP) Report
BTP Mode: ***On Campus***
Dhirubhai Ambani Institute of ICT (DA-IICT)
Gandhinagar, India
201901061@daiict.ac.in

Mentor's Name: Prof. Bhaskar Chaudhary
Dhirubhai Ambani Institute of ICT (DA-IICT)
Near Indroda Circle
Gandhinagar 382007, India
bhaskar_chaudhary@daiict.ac.in

***Abstract*—Imaging diagnostics provides valuable information about the behavior of plasma in various applications, such as tokamak fusion research and space propulsion systems. A tomographic reconstruction is a powerful tool for analyzing imaging diagnostic data and extracting information about plasma shape and position, impurity distribution, and Magneto-hydrodynamics (MHD) instabilities. However, the accuracy of the tomographic reconstruction is affected by the imaging diagnostic data. In this study, we propose a deep learning-based approach for reconstructing the 1D profile from synthetic 2D plasma images generated using imaging diagnostics. We first generate synthetic 2D plasma images using a 1D Gaussian profile as input. Then, we use a deep learning architecture to create a 2D Gaussian profile as output, which is used to extract the 1D profile. Our approach offers a more accurate and efficient way to reconstruct the 1D profile from synthetic 2D plasma images, which can improve the accuracy of tomographic reconstruction for plasma imaging diagnostics. The use of deep learning enables robust handling of reconstructing the synthetic imaging data, leading to more reliable and accurate tomographic reconstruction. The proposed method can contribute to the development of advanced plasma technologies and improve our understanding of plasma behavior. Overall, this study presents a novel approach for reconstructing the 1D profile from synthetic 2D plasma images using deep learning-based techniques. The proposed method has the potential to improve the accuracy and efficiency of tomographic reconstruction for plasma imaging diagnostics and contribute to the advancement of plasma technologies.**

***Index Terms*—MWCNN architecture, Reconstruction, 2D synthetic images, 2D emission images, 1D emission profile.**

I. Introduction

The quest for sustainable energy sources has become a pressing global challenge [1] [2]. Nuclear fusion, a process that produces energy by fusing atomic nuclei, holds tremendous promise as a clean, abundant, and safe alternative to traditional energy sources [3] [4]. Tokamak, a device that uses magnetic fields to confine high-temperature plasma, is one of the most promising architectures for achieving practical fusion power. However, the successful operation of a Tokamak requires a thorough understanding of the plasma dynamics, particularly the plasma shape and interior, which are critical to maintaining plasma stability and equilibrium.

To this end, imaging diagnostics has emerged as a vital tool in Tokamak plasma research. By capturing images of plasma across multiple wavelengths corresponding to different emission profiles, imaging diagnostics provides detailed monitoring of the plasma shape, emission profile shapes, and interior. Such information is critical for tomographic reconstructions, which can help recover plasma instabilities and modifications in the plasma emission profiles. However, extracting the necessary information from the final images remains a challenge.

This paper presents a comprehensive study of reconstructing the one-dimensional emission profile from a two-dimensional image, using machine learning algorithms. Specifically, the paper employs the MWCNN architecture, which takes synthetic two-dimensional images as input and generates a two-dimensional profile from a one-dimensional emission profile as output. The experimental setup for this study is described in detail in section II, which includes the viewing geometry, synthetic image generation, and two-dimensional profile generation. The proposed methods for reconstructing the one-dimensional emission profile are outlined in section III. Section IV presents the results and discussions, evaluating the performance of the proposed methods. Finally, section V summarizes the study's key findings, highlighting its contributions to Tokamak plasma diagnostics and its potential for advancing fusion energy research.

II. Experimental Setup

The experimental setup aimed at investigating the denoising of tokamak imaging diagnostics involves several crucial steps [5]. Firstly, the synthetic image needs to be generated, followed by the generation of the 2D profile image. Next, it is necessary to define the training and testing datasets for the model. The flowchart for experimental setup is shown in Fig. 1.

A. Synthetic Image Generation

The generation of synthetic images (SI) is the primary requirement for this study on tokamak plasma diagnostics. The SI is composed of a fundamental line-integrated emission information component, which is obtained along the line of sight for the camera pixels. [6]

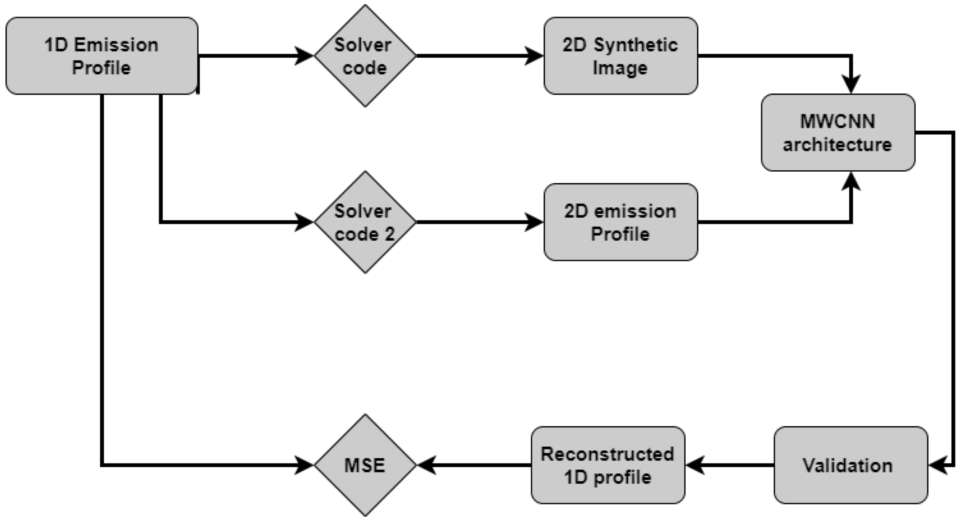

Fig. 1: Flowchat

This study focuses on a higher aspect ratio tokamak plasma, featuring a circular poloidal limiter, and up-down symmetry configuration. The plasma core temperature is sub keV, and the electron density is of the order of 10Î9 m≐3. To create the SI, a fast frame rate camera is utilized, which is situated at the plasma mid-plane and views the plasma tangentially, as presented in Figure 2. The camera encompasses 128x128 active pixels that span a total area of 1.25 inches x 1.25 inches on the sensor. The light collection process from the plasma to the camera sensor plane is performed using an optical assembly that avoids any issues with the dead space of the optical fiber bundles. The visible emission type of profile is of interest in this study and is of Gaussian nature. Fig 3 shows the 1D emission profile with a mean of 0.77 and a standard division of 0.115. This generated synthetic image is shown in Fig 4.

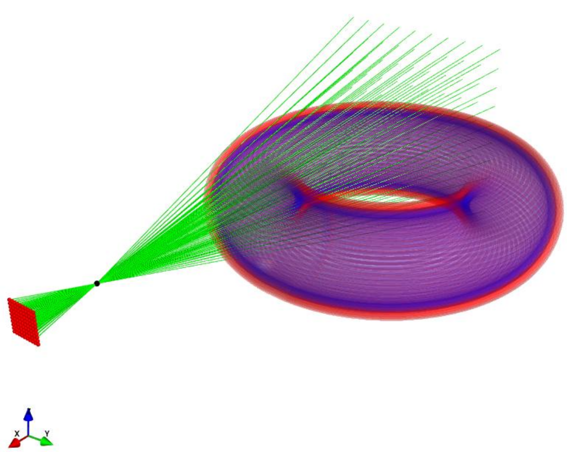
Fig. 2: Experiment setup for generating plasma image

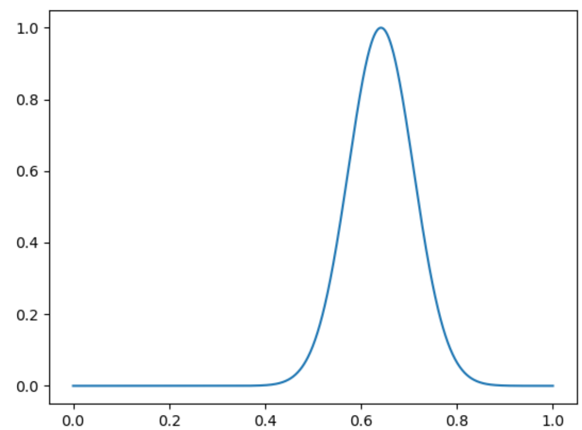

Fig. 3: 1D emission Profile

B. *2d profile generation*

To generate a 2D profile from a 1D profile, one approach is to map the 1D profile onto a 2D grid using some distance criterion. this is achieved by defining a circular region of interest around a center point and calculating the distance of each point on a 2D grid from the center point. If the distance is within the circular region, the 1D profile value is assigned to the corresponding point in the 2D grid. This results in a 2D profile that captures the spatial variation of the 1D profile.

Once the 2D profile is generated, it can be visualized using various techniques such as contour plots, surface plots, heatmaps, etc. A contour plot is used to visualize the 2D profile. This involves plotting the pressure values as contour lines on a 2D plane, where each contour line corresponds to a specific pressure level. The resulting plot provides a visual representation of the pressure distribution across the 2D region of interest, which is shown in Fig 5.

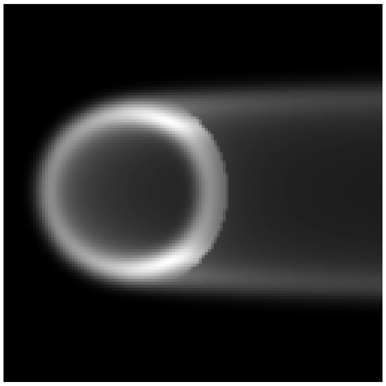

Fig. 4: 2D synthetic image

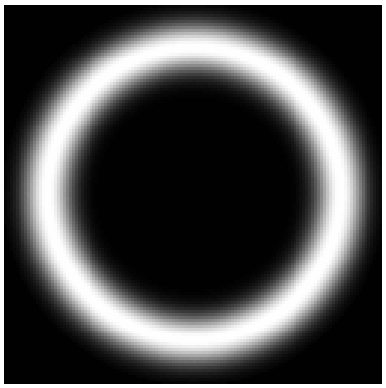

Fig. 5: 2D emission image

C. Evaluation Matrices

In image processing, evaluating the output images is crucial for assessing the performance of image reconstruction methods. A 2D Gaussian image is often used as a ground truth image (GTI), against which all output images are compared using metrics such as Peak Signal-to-Noise Ratio (PSNR) and Structural Similarity Index Measure (SSIM). In addition, the evaluation of the 1D reconstruction profile is commonly conducted using an absolute error function, which provides valuable insights into the accuracy of the reconstruction.

1) PSNR: PSNR is a widely used metric for evaluating signal reconstruction fidelity in the presence of noise, expressed in logarithmic units using the decibel scale due to the wide dynamic range of many signals, and commonly used in image and video compression applications. The utilization of PSNR provides a quantitative measure of the degree of similarity between the original and reconstructed signals, making it a crucial tool in many signal-processing applications.

$$PSNR = 10\log_{10}\left(\frac{255}{RMSE}\right)$$

Here, RMSE is Root Mean Squared Error.

2) SSIM: SSIM is a metric used to evaluate the perceptual difference between two images by measuring the similarity between their structures, providing a valuable tool in image processing applications. It is widely adopted in the field of image processing to provide a quantitative measure of the perceptual difference between two images.

$$SSIM = \frac{(2\mu_x\mu_y)(2\sigma_{xy}+c_2)}{(\mu_x^2+\mu_y^2)(\sigma_x+\sigma_y)}$$

Here, μ_x and μ_y are the mean intensity values of images x and y, σ_x^2 is the variance of x, σ_y^2 is the variance of y and σ_{xy}^2 is covariance of x and y.

3) Absolute error: In absolute error, we have calculated the difference between two 1d emission profiles which are reconstructed from the ground truth image and output image.

$$\text{Absolute Error} = \frac{1}{n}\sum_{i=1}^{n}|y_i - \hat{y}_i| \tag{1}$$

Here, y and $\hat{y}$ represented ground truth and output 1d profile respectively.

III. Proposed method

The MWCNN architecture is a powerful tool for image processing and classification tasks, and it can be used to process 2D synthetic plasma images and generate 2D emission profiles as output.

In this specific case, the input image is a 128x128 2D synthetic plasma image, which represents a simulated plasma state. The goal of the architecture is to learn the relevant features of the input image and generate a 2D emission profile that represents the emission intensity of the plasma at different locations. Some images from the training set are shown in Fig. 6.

A. Network Architecture

The MWCNN architecture (Fig. 5) employs a multi-scale wavelet transform to decompose the input image into frequency sub-bands, which are then processed by a convolutional neural network (CNN) at each level of decomposition. Each CNN block consists of four fully connected layers without pooling, taking all sub-band images as input. The architecture utilizes convolution, batch normalization, and rectified linear unit (ReLU) operations in each CNN layer. The last layer of the last CNN block predicts a residual image using convolution without batch normalization and ReLU. The overall architecture consists of a contracting and expanding subnetwork, which modifies the U-Net architecture by using discrete wavelet transforms and inverse wavelet transforms for downsampling and upsampling, respectively. The downsampling in MWCNN increases feature map channels, while the subsequent CNN blocks are used to reduce channels for compact representation. Element-wise summation is used to combine the feature maps from the contracting and expanding subnetworks. The final MWCNN network contains 24 layers. This architecture has achieved state-of-the-art performance in various image restoration tasks. [7]

The objective of learning the MWCNN architecture can be expressed as follows: Let Θ denote the set of network parameters and F(y; Θ) be the network output. Consider a training set (yi,xi), where yi is the ith input image and xi is

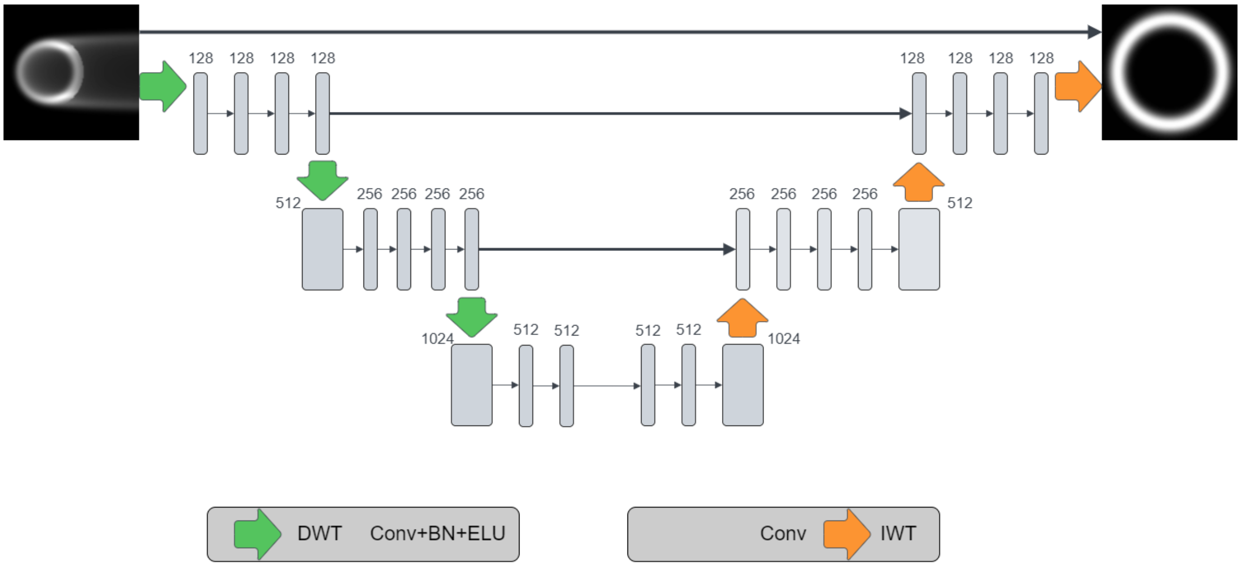

Fig. 6: MWCNN architecture

the corresponding ground-truth image. The objective function for learning the MWCNN is to minimize the error between the predicted output F(yi; Θ) and the ground-truth image xi, over the entire training set. This can be formulated as the minimization of a loss function L(Θ) defined as follows:

$$L(\Theta) = \frac{1}{N} \sum_{i=1}^{N} l(F(y_i; \Theta), x_i), \tag{2}$$

where N is the total number of training examples, and l(.) is a loss function that measures the discrepancy between the predicted output F(yi; Θ) and the ground-truth image xi. The objective is to find the values of Θ that minimize the loss function L(Θ). The RMSprop algorithm is adopted to train MWCNN by minimizing the objective function.

IV. Experiments

The purpose of this research study was to evaluate the effectiveness of 2D image reconstruction techniques. To accomplish this objective, an experiment was conducted, wherein the performance of various reconstruction methods was assessed. After obtaining the output images, a one-dimensional emission profile was reconstructed from each image.

A. Experimental setting

1) Training and testing dataset: To train the MWCNN for 2D image reconstruction, we constructed a large training set using synthetic plasma images. Specifically, we generated 704 synthetic images of size 128x128 pixels with varying emission profiles. The synthetic images were utilized to create a diverse and extensive training dataset for the MWCNN model. For testing, we used a separate set of 176 images.

The MWCNN was trained to learn a mapping from 2D synthetic images to 2D emission images, using the generated synthetic images as the input and the corresponding emission images as the target. This enabled the model to learn the underlying patterns and structures in the data, which allowed for the accurate reconstruction of emission images from new input data.

2) Network training: To learn the MWCNN model for each degradation setting, we utilized RMSprop optimization with a mini-batch size of 32 and a learning rate of 0.0005. We used the mean squared error (MSE) as the loss function for validation. All experiments were conducted on the Google Colab platform with GPU backend support. The learning algorithm converged rapidly, with each MWCNN model requiring approximately two hours for training. Our training process demonstrated effective optimization of the MWCNN models, allowing them to learn the underlying patterns and structures in the data and achieve high levels of accuracy in image reconstruction. The use of GPU acceleration also allowed for efficient and scalable training of the models.

B. Quantitative and qualitative evaluation

In this section, we used the same network setting described in 3.A.

1) One-to-One mapping: The trained network was evaluated on a test dataset, yielding an average peak signal-to-noise ratio (PSNR) of 38.91 and an average structural similarity index (SSIM) of 0.9842. These evaluation metrics indicate the promising performance of the network for the given task. Fig. 8 shows some images form training dataset.

2) Reconstuction of 1D Profile: Following the generation of output images, a 1D profile was reconstructed by slicing the middle row. Some of the resultant 1d profiles are shown in Fig. 9. Then the error between these two profiles is calculated by Absolute error.

V. Summary

In this research paper, we generated 2D synthetic data and a corresponding 2D emission profile. We then used a deep

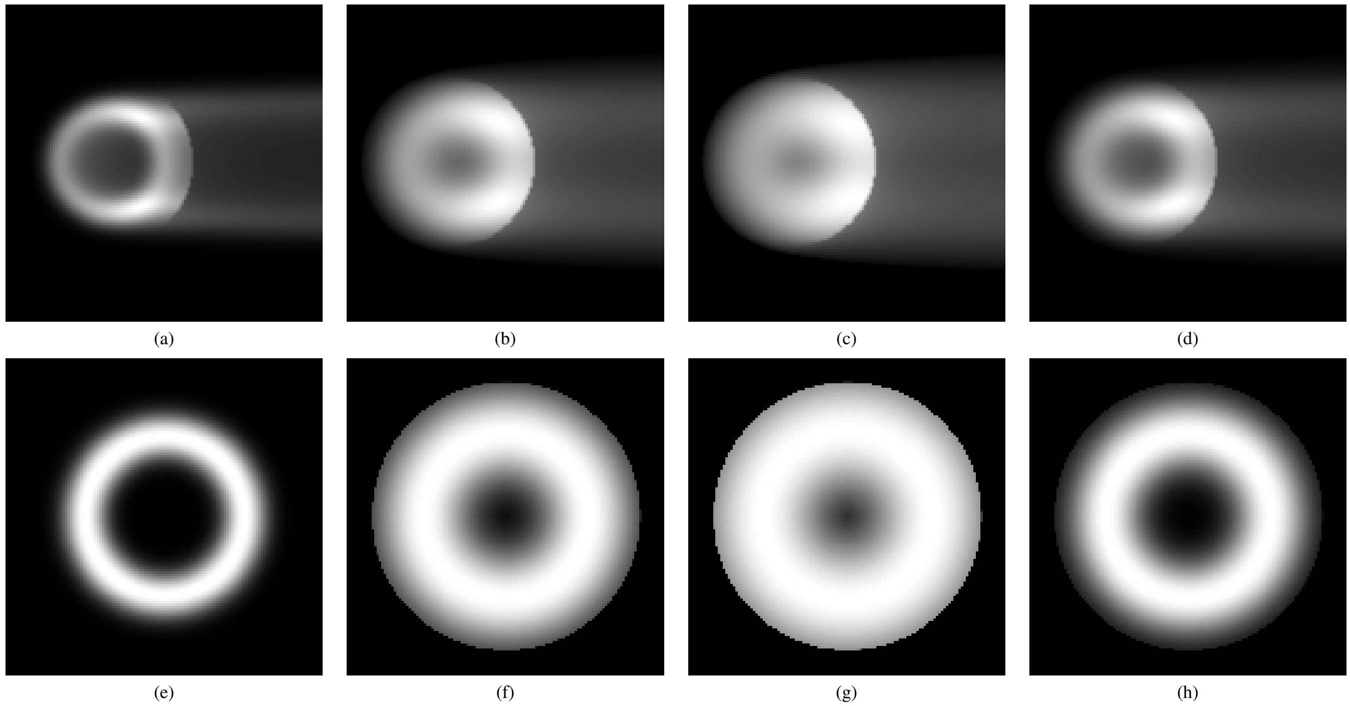

Fig. 7: (a), (b), (c), and (d) are 2d synthetic images generated with different 1d emission profiles. (e), (f), (g), and (h) are 2d emission profiles generated with different 1d emission profiles respectively.

learning architecture to perform one-to-one mapping between the 2D data and the emission profile. The predicted images were then used to reconstruct the 1D emission profile. The experimental results showed that the Multi-scale Wavelet Convolutional Neural Network (MWCNN) provided good results for this experiment. The error between the ground truth 1D profile and the predicted 1D profile was found to be low, indicating the effectiveness of the proposed approach.

Learning Outcome

In this research project, the first phase involved the acquisition of knowledge on image processing techniques. Subsequently, this knowledge was applied to generate two types of images: a 2D synthetic image and a 2D emission image. To further the project, a foundational understanding of deep learning architecture was attained, enabling the successful integration of the images into the model. Evaluation of the predicted images was then carried out using various matrices. Overall, this research project achieved its intended learning outcomes by providing a comprehensive understanding of image processing, deep learning architecture, and image evaluation techniques.

Contribution

The research project was conducted by me, with guidance provided by Prof. Bhaskar Chaudhury throughout the project. Dr. Shishir made a significant contribution by assisting in the generation of the 2D emission profile. Their valuable contributions helped to ensure the successful completion of the project. The acknowledgments of their contributions have been included in the research paper.

Acknowledgment

I would like to express my gratitude to Prof. Bhaskar Chaudhary from DAIICT and Dr. Shishir Purohit from the Institute for Plasma Research (IPR) for their valuable guidance and support throughout this research project. Their expertise and insights have been instrumental in shaping our work.

References

[1] Strachan, J. D., et al. ”High-temperature plasmas in a tokamak fusion test reactor.” Physical review letters 58.10 (1987): 1004.

[2] Strachan, J. D. ”Studies of global energy confinement in TFTR supershots.” Nuclear fusion 34.7 (1994): 1017.

[3] Keilhacker, M., et al. ”High fusion performance from deuterium-tritium plasmas in JET.” Nuclear Fusion 39.2 (1999): 209.

[4] Budny, R. V., et al. ”Core fusion power gain and alpha heating in JET, TFTR, and ITER.” Nuclear Fusion 56.5 (2016): 056002.

[5] Y. Nagayama, M. Yamada, W. Park, E. Fredrickson, A. Janos, K. McGuire, and G. Taylor, “Tomography of full sawtooth crashes on the tokamak fusion test reactor,” *Physics of Plasmas*, vol. 3, no. 5, pp. 1647–1655, 1996.

[6] K. Delwadia, D. Bhatt, S. Purohit, and B. Chaudhury, “Parallel algorithm for synthetic image generation with application to tokamak plasma diagnostics,” *Concurrency and Computation: Practice and Experience*, vol. 34, no. 24, p. e7217, 2022.

[7] P. Liu, H. Zhang, K. Zhang, L. Lin, and W. Zuo, “Multi-level wavelet-cnn for image restoration,” in *Proceedings of the IEEE conference on computer vision and pattern recognition workshops*, 2018, pp. 773–782.

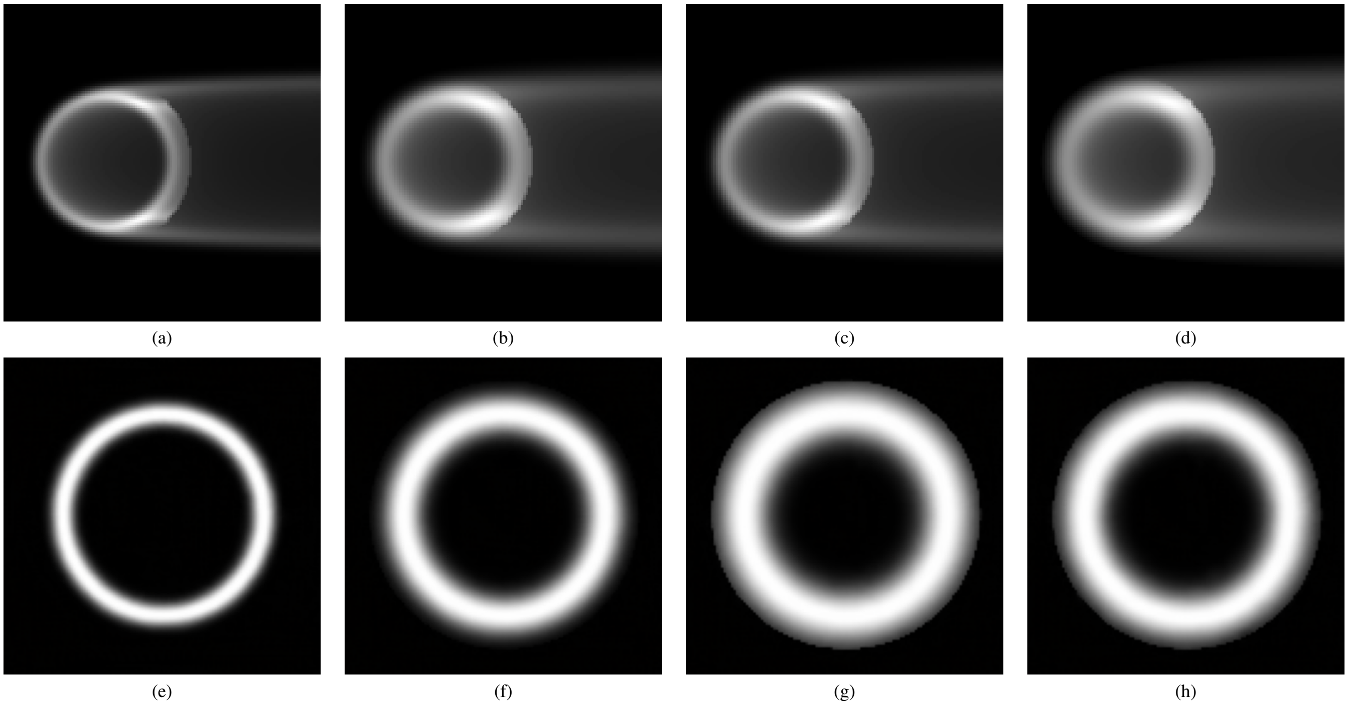

Fig. 8: (a), (b), (c), and (d) are 2d synthetic images generated. (e), (f), (g), and (h) are 2d emission profiles of (a), (b), (c), and (d) respectively.

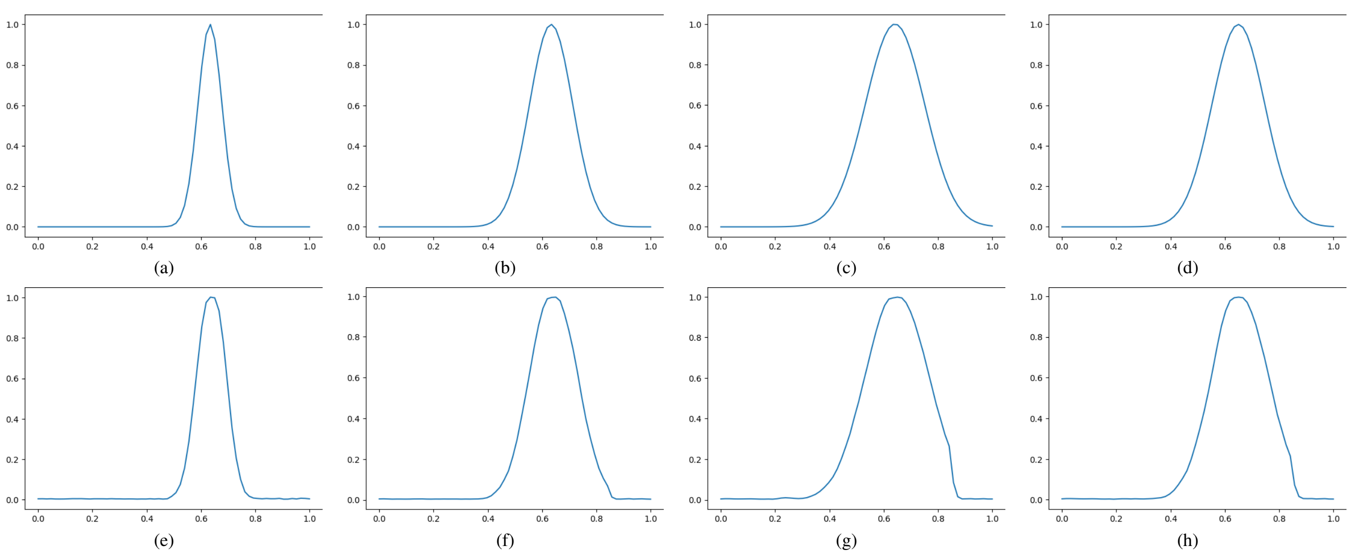

Fig. 9: (e), (f), (g), and (h) are predicted 1d profiles of (a), (b), (c), and (d) respectively.